Heat and Mass transfer on 3D Radiative MHD Casson Fluid Flow over a Stretching Permeable Sheet with Chemical Reaction and Heat Source/Sink

*R*avindra Kumar[1], *Sarook Khan*[1], *Deepak Kumar*[1] *and Sushila*[2*]
[1]*Department of Mathematics, Vivekananda Global University*,
Jaipur-303012, India
Email: rkmath1982@gmail.com, khansarook@gmail.com,deepak120786@gmail.com
[2]*Department of Physics, Vivekananda Global University*,
Jaipur-303012, India
Email: sushila.jag@gmail.com

Abstract

The objective of this research is to ascertain how 3D MHD heat transfer Casson fluid flow over a linearly porous stretched surface is affected by chemical reaction, radiation, and heat source/sink. The Roseland approximation is used to account for the radiation impact in the energy equation when examining the impacts of thermal radiation. Recently, there has been interest in heat transmission past a stretched sheet because of its numerous commercial applications and substantial impact on a variety of industrial processes. These consist of metal spinning, plastic sheet extrusion, condensation, heat exchangers, MHD generators, and power plants. The governing equations and related boundary conditions are reduced to a dimensionless form using similarity variables, and the Runge-Kutta-Fehlberg method is then used to solve the problem. An increase in the Casson fluid parameter, magnetic field parameter and Permeability parameter causes the velocity field to decrease in x and y directions and improve the temperature and concentration dispersion. Sherwood number and Skin friction coefficient over x and y direction are increasing function of Casson fluid parameter and Nusselt number is decreasing function while the reverse effect is seen in streatching sheet parameter. Nusselt number is increasing function of chemical reaction parameter, Schmidt number, Radiation parameter and heat heat source/sink parameters while the reverse effect is seen in Sherwood number.

Keywords: Chemical reaction, MHD Casson fluid , Stretching surface, Permeability, Heat Source/Sink.

1 Introduction:

The scientific literature has recently shown a great deal of interest in the vast array of biological uses for non-Newtonian fluids, including muds, low-shear rate blood, emulsions, apple sauce, sugar solutions, and shampoos. Fluids that do not flow in a Newtonian manner are referred to as non-Newtonian fluids. The International Atomic Energy Agency classifies them as actual non-Newtonian fluids that occur in nature. Numerous mathematical models have been proposed and examined in the

academic community, and many more are being developed. For instance, a greater variety of industrial applications employ Casson fluids. This model works well for researching the mechanics of yield-stress liquids with pseudo-plastic properties.[18] Thermal radiation, slip velocity, and MHD effects at the stagnation point flow across the stretched surface were examined. [15] the investigation of MHD in three dimensions of Casson fluid flow through a porous sheet that is linearly stretched is done. [9] focused on the impact of double dispersion, non-uniform heat source/sink, higher-order chemical processes, and MHD Casson fluid flow over a vertical cone and flat plate saturated with porous material on unstable, free convective flow. [21] A Casson fluid flow with magnetic nanoparticles incorporated is analyzed. It is believed that the flow is across a paraboloid of revolutions top surface. Nonlinear thermal radiation and viscous dissipation effects are taken into account. [29] examined the three-dimensional Newtonian and non-Newtonian MHD fluid flow. The investigation focuses on mass and heat transmission over a stretched surface when thermophoresis and Brownian motion are present. [6] Numerous biological activities, including the distribution of food, endoscopic procedures, the pumping of blood from the heart to different areas of the body, and the regulation of heat transport phenomena, depend heavily on multiple slips. [17] examined how heat, mass transport, and thermal radiation affected the three-dimensional Casson nanofluid's unstable MHD flow. Partial slip and convective circumstances might affect the flow. [22] examined the three-dimensional MHD Casson fluid flow across a stretched sheet using a non-Darcy porous material and a heat source/sink. [30] An unstable Casson fluid with mixed convection flow with slip and convective boundary conditions approaches a nonlinearly stretched sheet. Additionally examined are the impacts of Soret Dufour, viscous dissipation, and heat source/sink. [27] The effects of warm diffusion, chemical response, and heat radiation on the hydromagnetic pulsating flow of Casson fluid in a porous medium are investigated. [28] Investigations are conducted into the effects of heat radiation, chemical reactions, and thermal diffusion on the hydromagnetic pulsing flow of Casson fluid in a porous medium. [7] Discover the two-dimensional MHD movement of the Casson fluid and the dual solutions of heat transfer over the extension sheet. [14] aimed at describing the characteristics of melting heat transfer on Casson fluid flow in MHD flow in a porous medium under thermal radiation effect. [20] analyzed the impact of nonlinear thermal radiation with an non-uniform heat source and sink in the context of homogeneous-heterogeneous interactions on the three-dimensional Carreau and Casson fluid flow across a stretched surface in an unstable manner. [24] The study examines the consistent movement of a hybrid that is incompressible Casson nanofluid on an exponential stretching sheet that is permeable vertically.[8] The topic discussed is the unstable free convection slip flow of a second-grade fluid across an infinitely heated inclined plate. Additionally eligible are the impacts of mass diffusions in the flow. The constitutive equations for mass transport and heat employ the Caputo-Fabrizio fractional derivative, respectively.[26] examined the thin-film flow down an inclined plane of a third-grade fluid. The homotopy perturbation Elzaki transform technique is an efficient and well-organized computational methodology that is used to determine the solution of a nonlinear boundary value problem (BVP).[4] Single-walled carbon nanotubes are solid, microscopic materials found in nature that have good thermal conductivity and are valuable in many biological applications, particularly in the creation of biological nanofluid are examined.[12] investigated the features of heat transmission of a stationary 2D MHD Casson shear thickening liquid through a perpendicularly extended glass placed in a Variable heat sink/source combined with a permeable medium. [19] examined a rotating system's natural convection MHD Casson fluid flow via an oscillating vertical plate. Using a ramping wall temperature, the properties of thermal radiation, heat production, Hall current, and chemical reactions are examined. [23] examined how magneto-Casson nanofluid

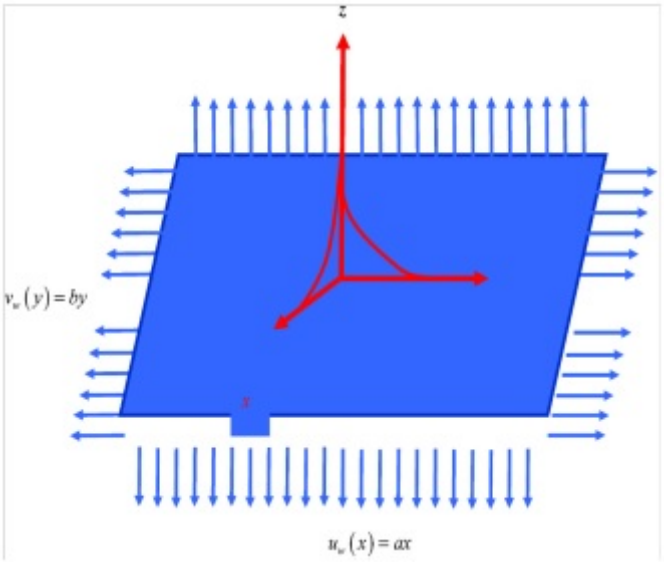

Figure 1: Schematic diagram of the Problem

phenomena, which result in thermal radiation passing through a porous inclined stretched sheet, are affected by chemical reactions and Joule heating. [25] Research was conducted under the stagnation zone to examine the heat and mass transfer of a hybrid nanomaterial Casson fluid with time-dependent flow across a vertical Riga sheet. With this formulation, Lorentz forces were introduced into the system when the Riga sheet was included in fluid flow models. [1] The investigation concentrated on the flow over a vertical stretching sheet near the stagnation point of a compressible, unstable Casson hybrid nanofluid flow. [5] achieved to uncover the novelty of a stretchable sheet with convective boundary conditions driving an incompressible MHD Casson liquid flow. [11] conducted a numerical investigation of the heat transfer of an electrically directed fluid across a radially extending sheet fixed in a permeable medium, as well as the axisymmetric mixed convection boundary layer flow. [16] examined the use of a vertically extended sheet embedded in a permeable material to explore MHDs varying convective stagnation point stream. [31] Measured the impact of radiation, Prandtl number, and chemical reaction on the Casson fluid flow during 3-D MHD heat transfer over a stretched surface with linear porosity. [2] The discussion focuses on Sutterby nanofluid flow at a nonlinear stretching cylinder with an induced magnetic field. Discussion is held on the impacts of viscous dissipation, Darcy resistance, and changing thermal conductivity. [3] Uncompressible We study Sutterby fluid flows across a cylinder that is stretched. When thermal slip, Darcy resistance, and sponginess are present, the impact of varying thermal conductivity is taken into account. [10] examined the effects of heat Source/Sink, joule heating, and thermal radiation on the two-dimensional nanofluid stagnation point flow above a stretched sheet anchored in a spongy medium. [13] Accessible properties include the transfer of melting heat through an exponentially stretched sheet placed in a porous material with a heat source and sink, as well as radiation and velocity slip on an MHD stream.

2 Construction of the Problem:

Consider the incompressible, electrically conducting steady 3D viscous Casson fluid movement on a surface that is extending. It is considered that the sheet is enlarged along xy-plane and stretched with velocities $U_w = ax$,$V_w = by$ in x- and y -directions (where a, b, are stretching constants), while the fluid is place along z-axis. let (u,v,w) denotes the components of velocity along the (x,y,z) paths correspondingly. The physical coordinate system and geometry of this model are exposed in Fig. 1. The Hall current and the Joule dissipation are not taken into consideration and both the consequences of chemical response and the effects of radiation are taken into account.The rheological equation of a Casson fluid can be articulated as

$$\begin{aligned} \tau_{ij} &= 2\left(\mu_B + \frac{p_z}{\sqrt{2\pi}}\right) e_{ij}, \pi > \pi_c \\ &= 2\left(\mu_B + \frac{p_z}{\sqrt{2\pi_c}}\right) e_{ij}, \pi < \pi_c \end{aligned} \tag{1}$$

where $\pi = e_{ij}e_{ji}$, e_{ij} is the (i,j)ˆth component of the deformation rate with itself, π_c is the decisive value of this product based on the shear thickening model, μ_B is the plastic dynamic viscosity of Casson fluid, and p_y is the yield stress of the fluid Equation of Continuity

$$\frac{\partial u}{\partial x} + \frac{\partial v}{\partial y} + \frac{\partial w}{\partial z} = 0, \tag{2}$$

Equation of Momentum

$$u\frac{\partial u}{\partial x} + v\frac{\partial u}{\partial y} + w\frac{\partial u}{\partial z} = \nu\left(1 + \frac{1}{\beta}\right)\frac{\partial^2 u}{\partial z^2} - \frac{\sigma {B_0}^2 u}{\rho} - \frac{\nu}{k}u, \tag{3}$$

$$u\frac{\partial v}{\partial x} + v\frac{\partial v}{\partial y} + w\frac{\partial v}{\partial z} = \nu\left(1 + \frac{1}{\beta}\right)\frac{\partial^2 v}{\partial z^2} - \frac{\sigma {B_0}^2 v}{\rho} - \frac{\nu}{k}v, \tag{4}$$

Equation of Energy

$$\begin{aligned} u\frac{\partial T}{\partial x} + v\frac{\partial T}{\partial y} + w\frac{\partial T}{\partial z} &= \frac{k}{\rho C_p}\frac{\partial^2 T}{\partial z^2} - \frac{1}{\rho c_p}\frac{\partial q_r}{\partial z} \\ +\tau\left(D_b\frac{\partial T}{\partial y}\frac{\partial C}{\partial y} + \frac{D_T}{T_\infty}\left(\frac{\partial T}{\partial y}\right)^2\right) &+ \frac{Q^*(T - T_\infty)}{\rho c_p} \end{aligned} \tag{5}$$

Equation of Species Diffusion

$$u\frac{\partial C}{\partial x} + v\frac{\partial C}{\partial y} + w\frac{\partial C}{\partial z} = D_b\frac{\partial^2 C}{\partial z^2} + \frac{D_T}{T_\infty}\frac{\partial^2 T}{\partial z^2} - {C_r}^*\left(C - C_\infty\right) \tag{6}$$

The boundary conditions for this flow are

$$\begin{gathered} u = u_w(x) = ax, v = V_w(x) = by, C = C_w, T = T_w, at\ z = 0, and \\ u \to 0, v \to 0,\ \ T \to T_\infty, C \to C_\infty, as\ z \to \infty \end{gathered} \tag{7}$$

The radiative heat flux, according to the Rosseland's estimate, is

$$q_r = -\frac{4}{3}\frac{\sigma^*}{k^*}\frac{\partial T^4}{\partial z} \tag{8}$$

Where the Stefan-Boltzmann constant σ^* and the mean absorption coefficient k^*, respectively, are the values. The growth of T^4 near T_∞ in the Tailor series is

$$T^4 = 4TT_\infty{}^3 - 3T_\infty{}^4 \tag{9}$$

Now let us utilize the ensuing similarity conversions
The velocity components can be defined as follows in terms of the stream function ψ as

$$\begin{gathered}\eta = \sqrt{\frac{a}{\nu}}y\ , u = axf'(\eta),\ v = byg'(\eta),\ ,\ w = -\sqrt{a\nu}(f(\eta)+cg(\eta)) \\ \theta(\eta) = \frac{(T-T_\infty)}{(T_w-T_\infty)}, \phi(\eta) = \frac{(C-C_\infty)}{(C_w-C_\infty)}\end{gathered} \tag{10}$$

Here $c = \frac{b}{a}$, is the velocity ratio among the x and y axes, and ($\hat{}$) denotes diff. w. r. to η
By use of Eq. (8), (9), and (10), Eqs. (3), (4), (5), and (6) take the below form

$$\left(1+\frac{1}{\beta}\right)f''' + (f+cg)f'' - f'^2 - (M+K)f' = 0, \tag{11}$$

$$\left(1+\frac{1}{\beta}\right)g''' + (f+cg)g'' - cg'^2 - (M+K)g' = 0, \tag{12}$$

$$(1+Ra)\theta'' + Pr[Nb\theta'\phi' + Nt\theta'^2 + (f+cg)\theta' + \delta\theta] = 0 \tag{13}$$

$$\phi'' + \frac{Nt}{Nb}\theta'' + Sc\left[(f+cg)\phi' - Cr\phi\right] = 0, \tag{14}$$

the corresponding boundary conditions (7) become

$$\begin{gathered}f(0)=0, g(0)=0, f'(0)=1, g'(0)=c, \theta(0)=1, \phi(0)=1, \\ f'(\infty)\to 0, g'(\infty)\to 0, \theta(\infty)\to 0, \phi(\infty)\to 0,\end{gathered} \tag{15}$$

with respect to the relevant physical characteristics
where $M = \frac{\sigma {B_0}^2}{\rho a}$, hint to the magnetic restriction, $K = \frac{\nu}{ka}$ is the permeability parameter, $Pr = \frac{\nu}{\alpha}$ is Prandtl number, $Ra = \frac{16\sigma^* {T_\infty}^3}{3kk^*}$ is radiation parameter, $Nb = \frac{\tau D_b(C_w-C_\infty)}{\nu}$ shows the Brownian motion parameter, $Nt = \frac{\tau D_T(T_w-T_\infty)}{\nu T_\infty}$ is thermophoresis parameter, $\delta = \frac{Q^*}{\rho C_p U_w}$ heat source/sink, parameter, $Sc = \frac{\nu}{D_b}$ Schmidt number, and $Cr = \frac{{C_r}^*}{a}$ is the chemical reaction.
Quantities of physical interest, the physical parameters of the friction factor over x, y paths, and the Nusselt number and Sherwood numbers are shown.

$$C_{f_x} = \frac{\tau_{wx}}{\rho {U_w}^2} \Rightarrow C_{f_x}{Re_x}^{\frac{1}{2}} = \left(1+\frac{1}{\beta}\right)f''(0) \tag{16}$$

$$C_{f_y} = \frac{\tau_{wy}}{\rho {V_w}^2} \Rightarrow C_{f_y}{Re_y}^{\frac{1}{2}} = \left(1+\frac{1}{\beta}\right)\frac{1}{c}g''(0) \tag{17}$$

$$Nu_x = \frac{xq_w}{k(T_w-T_\infty)} \Rightarrow Nu_x{Re_x}^{\frac{-1}{2}} = -\theta'(0) \tag{18}$$

$$Sh_x = \frac{xq_m}{D_b(C_w-C_\infty)} \Rightarrow Sh_x{Re_x}^{\frac{-1}{2}} = -\phi'(0) \tag{19}$$

where

$$q_w = -k\left(\frac{\partial T}{\partial z}\right)_{z=0}, q_m = -\left(D_b\frac{\partial C}{\partial z}\right)_{z=0} \tag{20}$$

$Re_x = \frac{xU_w}{\nu}$ and $Re_y = \frac{yV_w}{\nu}$ are the local Reynolds numbers.

Mathematical process for result:
The result of equations. (11), (12), (13), and (14) jointly through borderline circumstances (15) is determined through a systematic numerical method be aware shooting technique. We translate the nonlinear equivalences into first-order regular differential equivalences by labeling the variable quantity i.e.
$f = f_1, f^{'} = f_2, f^{''} = f_3, g = f_4, g^{'} = f_5, g^{''} = f_6, \theta = f_7, \theta^{'} = f_8, \phi = f_9, \phi^{'} = f_10,$
Hence, the system of equations becomes

$$f_1^{'} = f_2, \tag{22}$$

$$f_2^{'} = f_3, \tag{23}$$

$$f_3^{'} = \left(1+\frac{1}{\beta}\right)^{-1}[f_2^2 - (f_1+cf_4)f_3 + (M+K)f_2] \tag{24}$$

$$f_4^{'} = f_5, \tag{25}$$

$$f_5^{'} = f_6, \tag{26}$$

$$f_6^{'} = \left(1+\frac{1}{\beta}\right)^{-1}[cf_5^2 - (f_1+cf_4)f_6 + (M+K)f_5] \tag{27}$$

$$f_7^{'} = f_8, \tag{28}$$

$$f_8^{'} = (1+Ra)^{-1}[Nbf_8f_{10} + Nt{f_8}^2 + (f_1+cf_4)f_8 + \delta f_7] \tag{29}$$

$$f_9^{'} = f_{10}, \tag{30}$$

$${f_{10}}^{'} = Sc[Crf_9 - (f_1+cf_4)f_{10}] - \frac{Nt}{Nb}f_8^{'}, \tag{31}$$

Subject to the following conditions

$$f_1(0)=0, f_2(0)=1, f_3(0)=S_1, f_4(0)=0, f_5(0)=c, f_6(0)=S_2, f_7(0)=1, \\ f_8(0)=S_3, f_9(0)=0, f_{10}(0)=S_4, \tag{32}$$

$$f_2(\infty)=0, f_4(\infty)=0, f_6(\infty)=0, f_8(\infty)=0,\ as\ \eta\to\infty \tag{33}$$

Now Runge Kutta Fehlberg (RKF45) for stepwise integration, a numerical technique with shooting method is used, and MATLAB software is used for the computations.

3 Results and discussion

Figs. 2, 3, 4, and 5 show how the magnetic parameter affects velocity along the x- and y-directions, temperature, and concentration. Here, we observed that the temperature and concentration increased as they increased, but the velocity profile decreased. It has been observed that a stronger magnetic field makes flow more difficult. The momentum boundary layer thickness decreased as a result of the change in velocity profile, as illustrated in Figs. 2 and 3.

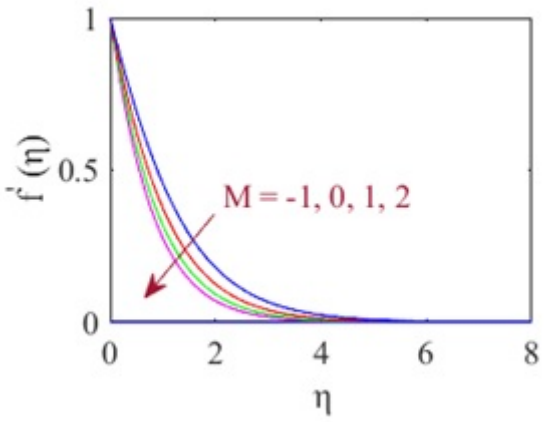

Figure 2: Behaviour of the magnetic parameter M on velocity along the x direction.

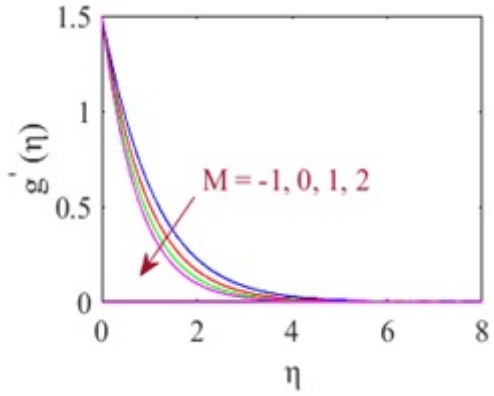

Figure 3: Behaviour of the magnetic parameter M on velocity along the y direction.

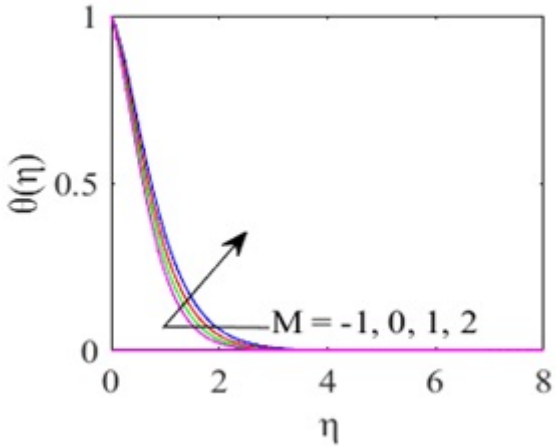

Figure 4: Behaviour of the magnetic parameter M on temperature.

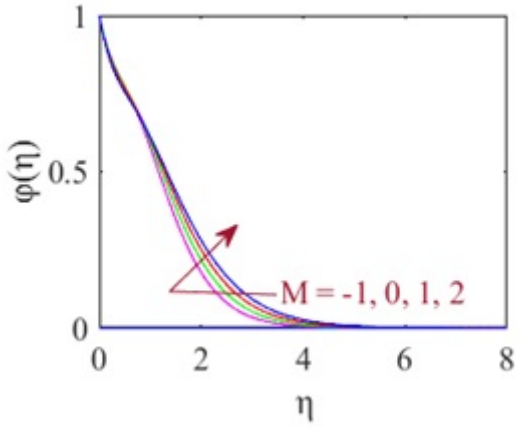

Figure 5: Behaviour of the magnetic parameter M on concenteration.

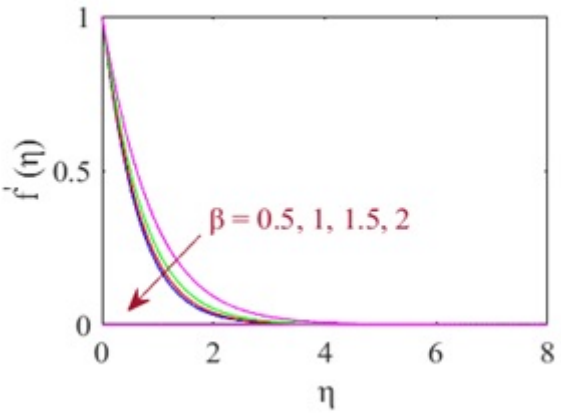

Figure 6: Behaviour of the Casson fluid parameter β on velocity along the x direction.

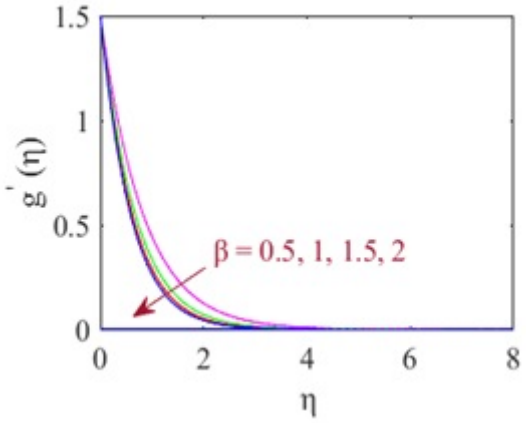

Figure 7: Behaviour of the Casson fluid parameter β on velocity along the y direction.

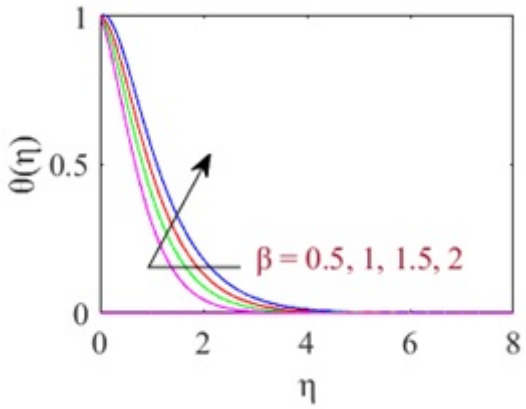

Figure 8: Behaviour of the Casson fluid parameter β on temperature.

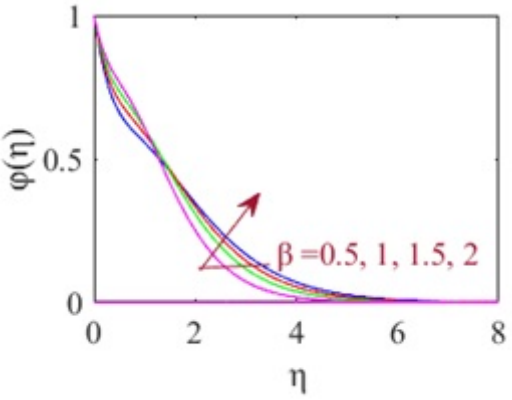

Figure 9: Behaviour of the Casson fluid parameter β on concenteration.

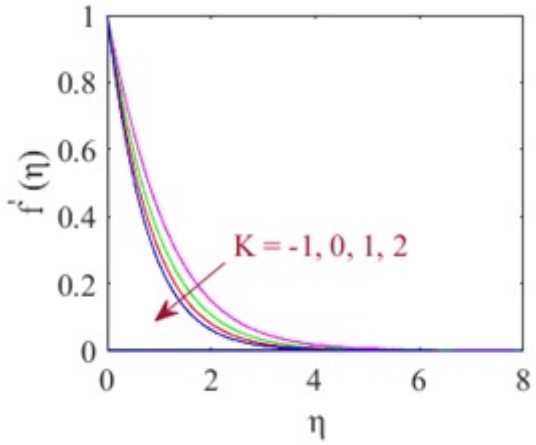

Figure 10: Behaviour of the permeability parameter K velocity along the x direction.

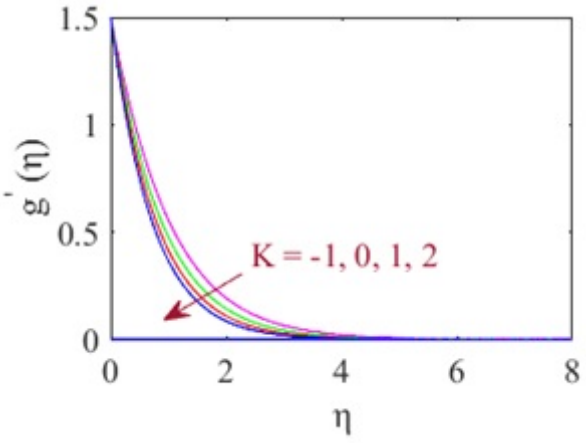

Figure 11: Behaviour of the permeability parameter K velocity along the y direction.

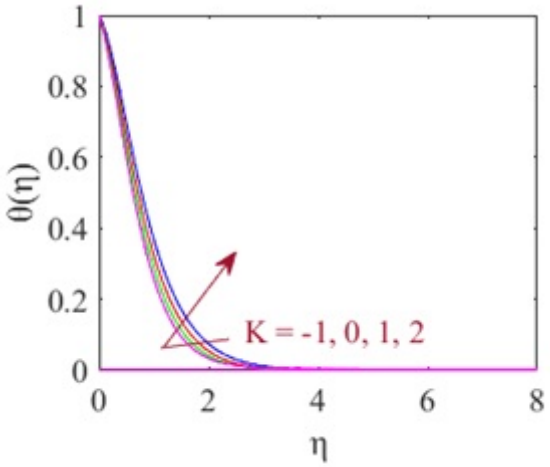

Figure 12: Behaviour of the permeability parameter K on temperature.

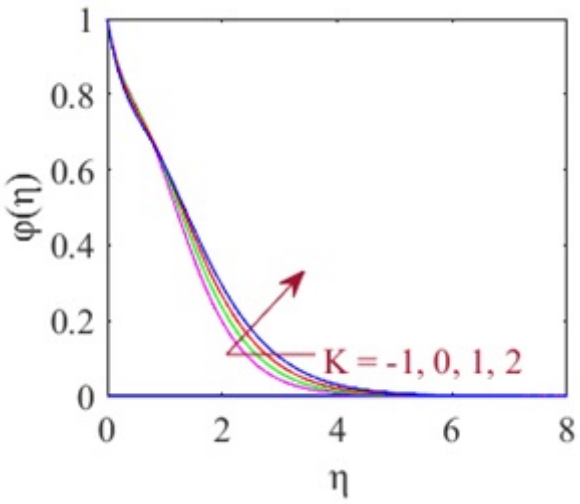

Figure 13: Behaviour of the permeability parameter K on concentration.

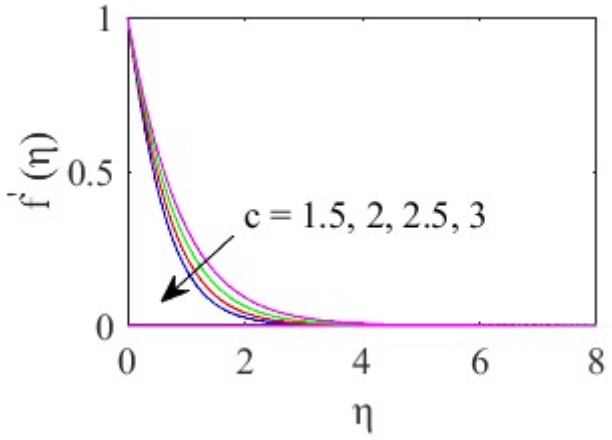

Figure 14: Behaviour of the Stretching sheet parameter c on velocity along the x direction.

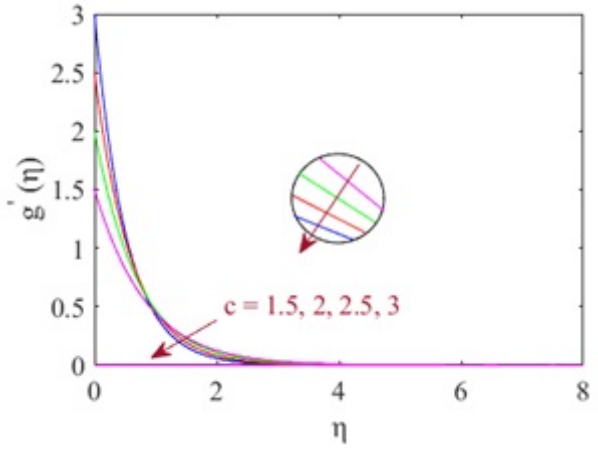

Figure 15: Behaviour of the Stretching sheet parameter c on velocity along the y direction.

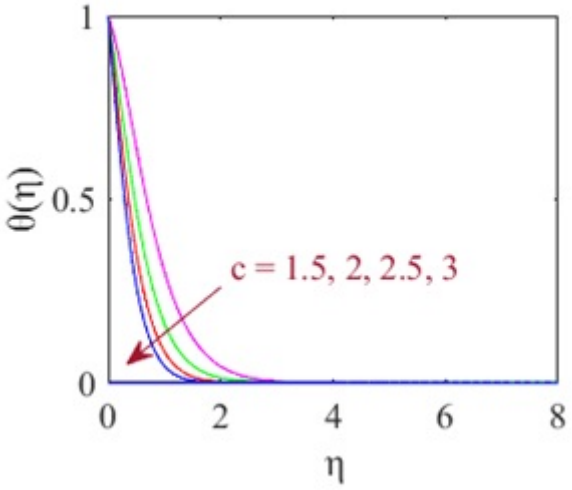

Figure 16: Behaviour of the Stretching sheet parameter c on temperature.

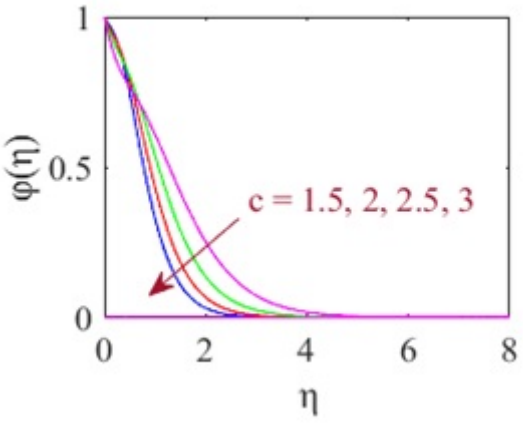

Figure 17: Behaviour of the Stretching sheet parameter c on on concenteration.

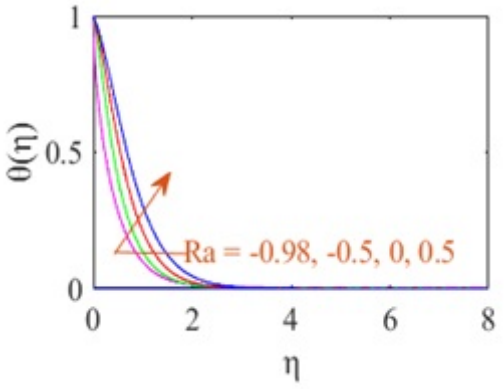

Figure 18: Behaviour of the radiation parameter Ra on temperature.

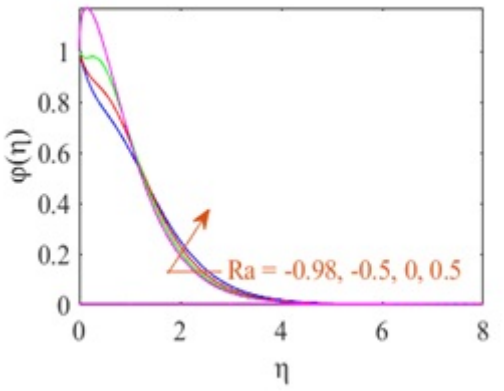

Figure 19: Behaviour of the radiation parameter Ra on concenteration.

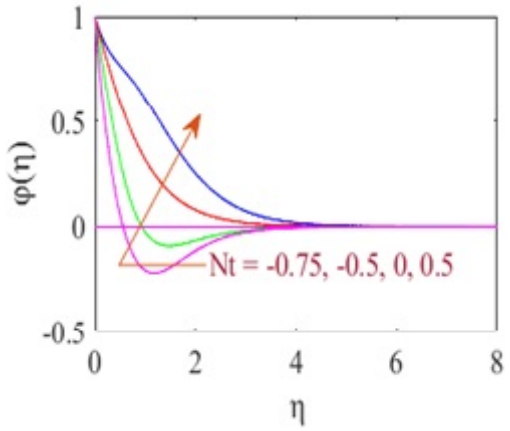

Figure 20: Thermoplastics parameter Nt behavior with respect to temperature.

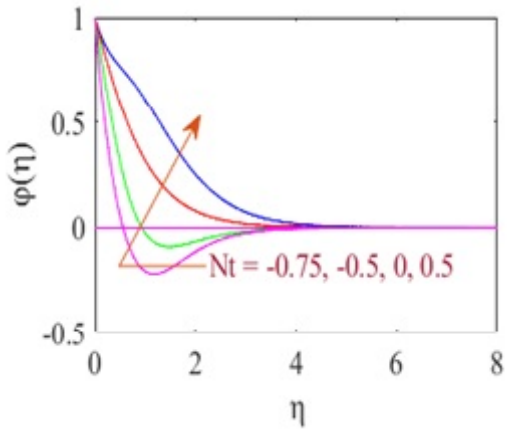

Figure 21: Behaviour of the thermophoresis parameter Nt on concentration.

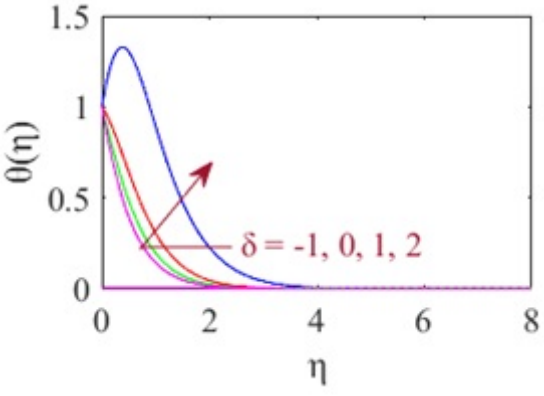

Figure 22: Behaviour of the heat source/sink parameter δ on temperature.

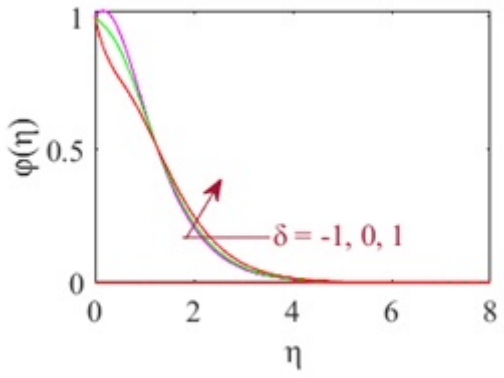

Figure 23: Behaviour of the heat source/sink parameter δ on concentration.

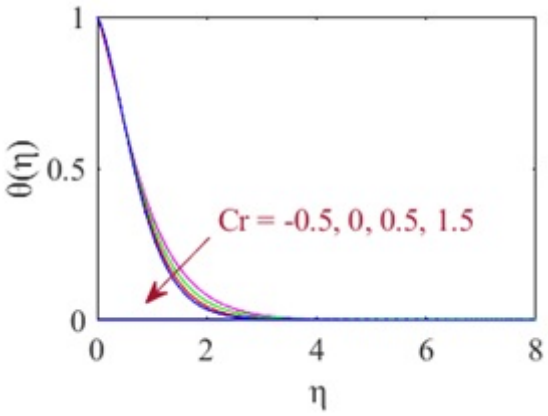

Figure 24: Behaviour of the chemical reaction Cr on temperature.

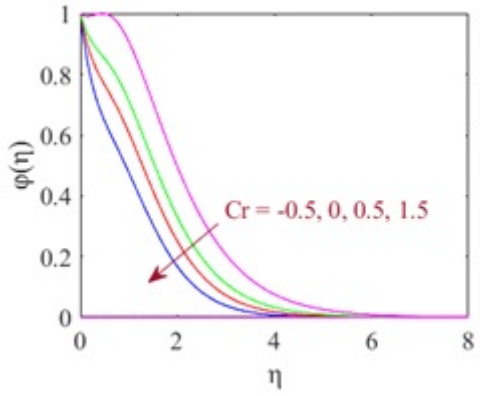

Figure 25: Behaviour of the chemical reaction Cr on concentration.

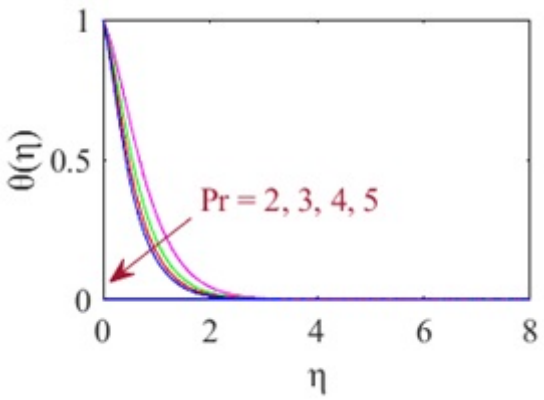

Figure 26: Behaviour of the Prandtl number Pr on temperature.

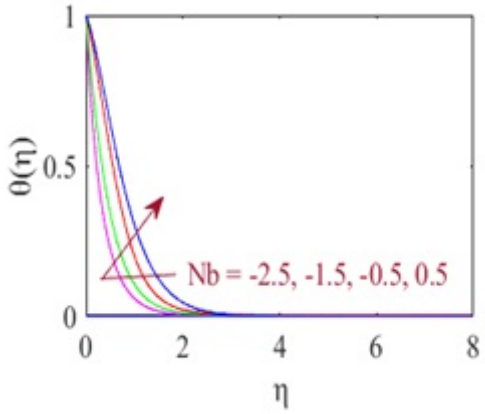

Figure 27: Behaviour of the Brownian motion restriction Nb on concentration.

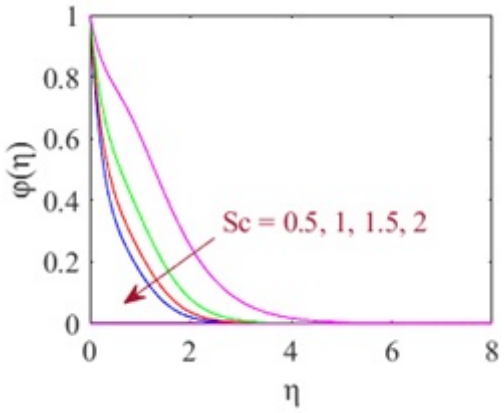

Figure 28: . Behaviour of the Schmidt number Sc on on concentration.

Table 1: Impact of different non-dimensional controlling factors on friction factors C_{f_x}, C_{f_y}, Nusselt number N_{u_x} and Sherwood number S_{u_x}.

Parameter	C_{f_x}	C_{f_y}	N_{u_x}	S_{u_x}
$M = -1$	-2.005746	-2.544402	0.580582	0.801173
$M = 0$	-2.629326	-3.064782	0.500582	0.818533
$M = 1$	-3.140856	-3.51485	0.417652	0.848203
$M = 2$	-3.583068	-3.915582	0.326602	0.891835
$K = -1$	-2.334816	-2.815062	0.521082	0.823045
$K = 0$	-2.895696	-3.297062	0.451682	0.838045
$K = 1$	-3.368973	-3.720438	0.372052	0.869313
$K = 2$	-3.785391	-4.101684	0.275052	0.920523
$\beta = 0.5$	-3.140856	-3.51485	0.417652	0.848203
$\beta = 1$	-2.564498	-2.8698667	0.208992	0.958713
$\beta = 1.5$	-2.341055	-2.6198178	0.044302	1.066831
$\beta = 2$	-2.2209195	-2.485376	-0.1243	1.189151
$c = 1.5$	-3.140856	-3.51485	0.417652	0.848203
$c = 2$	-3.416166	-4.199868	0.931302	0.608003
$c = 2.5$	-3.738744	-4.9411452	1.375402	0.448203
$c = 3$	-4.097244	-5.717001	1.775402	0.338553

Table 2: Impact of different non-dimensional controlling factors on Nusselt number N_{u_x} and Sherwood number S_{u_x}.

Parameter	N_{u_x}	S_{u_x}
$Pr = 2$	0.417652	0.848203
$Pr = 3$	0.573052	0.740903
$Pr = 4$	0.703052	0.641503
$Pr = 5$	0.830052	0.537983
$Cr = -0.5$	0.510152	0.121503
$Cr = 0$	0.457652	0.556253
$Cr = 0.5$	0.417652	0.848203
$Cr = 1$	0.307652	1.307885
$Sc = 0.5$	0.417652	0.848203
$Sc = 1$	0.155712	1.617803
$Sc = 1.5$	-0.05071	2.188503
$Sc = 2$	-0.18071	2.632103
$Ra = -0.98$	9.510052	-8.020473
$Ra = -0.5$	0.915052	0.466403
$Ra = 0$	0.580052	0.735203
$Ra = 0.5$	0.417652	0.848203
$\delta = -1$	1.658502	-0.259983
$\delta = 0$	1.152222	0.197903
$\delta = 1$	0.417652	0.848203
$\delta = 2$	-1.75765	2.671003
$Nb = -2.5$	3.325092	1.469253
$Nb = -1.5$	1.957652	1.404003
$Nb = -0.5$	0.657652	1.183203
$Nb = 0.5$	0.417652	0.848203
$Nt = -0.75$	1.940152	3.092603
$Nt = -0.5$	1.007152	1.500203
$Nt = 0$	0.512552	0.920423
$Nt = 0.5$	0.417652	0.848203

Higher values result in a larger Lorentz force in the magnetic field, which increases the thickness of the thermal boundary layer. Evidently, the Lorentz force is generated by a magnetic field with antagonistic/resistive strength. That causes the fluid velocity to decrease and causes the flow boundary layer to narrow. Figs. 6, 10, 7, 11, 8, 9, and 12, 13 show how Casson fluid parameter and permeability parameter affect velocity along the x- and y-directions, temperature, and concentration. Here, we observed that in figures 8, 9, and 12, 13, the temperature and concentration increased as they increased, but in figures 6, 10, and 7, 11 the velocity profile decreased because the yield stress of the fluid is represented by the Casson fluid parameter. The lowest tension that a fluid has to have in order to flow is known as yield stress. With an increase in the Casson fluid parameter, the fluid yield stress decreases and its viscosity increases. The velocity decreases more gradually as a result. Figs. 14, 15, 16, and 17 show how the stretching sheet parameter affects velocity along the x- and y-directions, temperature, and concentration. Here, we observed that the velocity along the x- and y-directions, temperature, and concentration increased as they increased. Figs. 18, 19, 20, 21, 22, and 23 shows how the radiation parameter, thermophoresis parameter, and heat source/sink parameter affect temperature and concentration. Here, we observed that the temperature and concentration increased as increased, and a reverse effect is seen in Figs. 24 and 25 for chemical reactions. Fig. 26 shows how the Prandtl number affects temperature. Here, we observed that the temperature decreased as it increased.When heat is transferred in relation to momentum, a higher Prandtl number denotes slower heat transfer, and a lower Prandtl number implies faster heat transfer. A fluid with a high Prandtl number often has a relatively short temperature gradient and a smooth, well-mixed temperature profile. Figs. 27 and 28 show how the Brownian motion parameter and Schmidt number affect concentration. Here, we observed that concentration increased as the Brownian motion parameter increased, and a reverse effect is seen in the Schmidt number.

4 Conclusions

This study investigated the effects of radiation and the Prandtl number on the three-dimensional Casson fluid flow across a stretched surface when a magnetic field is present with chemical reaction, and heat source/sink. Prior to being numerically solved, this model is transformed and compressed into a dimensionless form. The numerical data has been used to create graphs and tables that show the flow characteristics.
The principal conclusions drawn from this study are:

- An increase in the magnetic field parameter, Casson fluid parameter, and permeability parameter leads to a decrease in the velocity field in the x and y directions and enhances the distribution of temperature and concentration.
- Increase in Stretching the sheet parameter increases the temperature, concentration, and velocity field in the x and y directions.
- An increase in the radiation parameter, heat source/sink parameter, and thermophoresis parameter increases temperature and concentration, and a reverse effect is seen in the chemical reaction parameter.
- Increase in stretching sheet parameter decrease in temperature, concentration, and velocity field in x and y directions.
- An increase in Prandtl number decreases the temperature.
- An increase in the Schmidt number decreases the concentration.

- The Nusselt number and skin friction coefficient over x and y directions are decreasing functions, while the Sherwood number is an increasing function of the magnetic field parameter and radiation parameter.
- Sherwood number and skin friction coefficient over x and y directions are increasing functions of the Casson fluid parameter, and Nusselt number is a decreasing function, while the reverse effect is seen in the stretching sheet parameter.
- The Nusselt number is an increasing function of the chemical reaction parameter, Schmidt number, radiation parameter, and heat source/sink parameters, while the reverse effect is seen in the Sherwood number.
- The Nusselt number and the Sherwood number are both decreasing functions of the Brownian motion parameter and the thermophoresis parameter.

[1] [2] [3] [5] [6] [7] [9] [12] [11] [13] [10] [14] [15] [16] [17] [18] [19] [20] [21] [22] [23] [24] [25] [27] [28] [29] [30] [31] [4] [26] [8]

References

[1] Abbas, N., Shatanawi, W., and Abodayeh, K. Computational analysis of mhd nonlinear radiation casson hybrid nanofluid flow at vertical stretching sheet. *Symmetry 14*, 7 (2022), 1494.

[2] Abbas, N., Shatanawi, W., Hasan, F., and Shatnawi, T. A. Numerical analysis of darcy resistant sutterby nanofluid flow with effect of radiation and chemical reaction over stretching cylinder: induced magnetic field. *AIMS Math 8* (2023), 11202–11220.

[3] Abbas, N., Shatanawi, W., Shatnawi, T. A., and Hasan, F. Theoretical analysis of induced mhd sutterby fluid flow with variable thermal conductivity and thermal slip over a stretching cylinder. *AIMS Mathematics 8*, 5 (2023), 10146–10159.

[4] Ahmad, M., Asjad, M. I., and Singh, J. Application of novel fractional derivative to heat and mass transfer analysis for the slippage flow of viscous fluid with single-wall carbon nanotube subject to newtonian heating. *Mathematical Methods in the Applied Sciences* (2021).

[5] Anantha Kumar, K., Venkata Ramudu, A., Sugunamma, V., and Sandeep, N. Effect of non-linear thermal radiation on mhd casson fluid flow past a stretching surface with chemical reaction. *International Journal of Ambient Energy 43*, 1 (2022), 8400–8407.

[6] Gopal, D., Kishan, N., and Raju, C. Viscous and joule's dissipation on casson fluid over a chemically reacting stretching sheet with inclined magnetic field and multiple slips. *Informatics in medicine Unlocked 9* (2017), 154–160.

[7] Hamid, M., Usman, M., Khan, Z., Ahmad, R., and Wang, W. Dual solutions and stability analysis of flow and heat transfer of casson fluid over a stretching sheet. *Physics Letters A 383*, 20 (2019), 2400–2408.

[8] Haq, S. U., Jan, S. U., Shah, S. I. A., Khan, I., and Singh, J. Heat and mass transfer of fractional second grade fluid with slippage and ramped wall temperature using caputo-fabrizio fractional derivative approach. *AIMS Mathematics 5*, 4 (2020), 3056–3088.

[9] Jasmine Benazir, A., Sivaraj, R., and Makinde, O. D. Unsteady magnetohydrodynamic casson fluid flow over a vertical cone and flat plate with non-uniform heat source/sink. *International Journal of Engineering Research in Africa 21* (2016), 69–83.

[10] Kumar, R., Mehta, R., Mehta, T., et al. Mhd stagnation point flow and heat transfer of a nanofluid over a stretching sheet fixed in porous medium with effect of thermal radiation, joule heating and heat source/sink. *Journal of Computational Analysis & Applications 31*, 1 (2023).

[11] Kumar, R., Mehta, R., Rathore, H., and Kumar, M. Effect of axisymmetric mixed convection boundary layer flow and heat transmission over exponentially stretching sheet fixed in porous medium with heat source/sink and radiation effect. *International Journal of Energy for a Clean Environment 23*, 7 (2022).

[12] Kumar, R., Mehta, R., Sharma, K., and Kumar, D. Effect of suction/injection on the stream of a magnetohydrodynamic casson fluid over a vertical stretching surface installed in a porous medium with a variable heat sink/source. *Science & Technology Asia* (2021), 13–26.

[13] Kumar, R., Singh, J., Mehta, R., Kumar, D., and Baleanu, D. Analysis of the impact of thermal radiation and velocity slip on the melting of magnetic hydrodynamic micropolar fluid-flow over an exponentially stretching sheet. *Thermal Science 27*, Spec. issue 1 (2023), 311–322.

[14] Mabood, F., and Das, K. Outlining the impact of melting on mhd casson fluid flow past a stretching sheet in a porous medium with radiation. *Heliyon 5*, 2 (2019).

[15] Mahanta, G., and Shaw, S. 3d casson fluid flow past a porous linearly stretching sheet with convective boundary condition. *Alexandria Engineering Journal 54*, 3 (2015), 653–659.

[16] Mehta, R., Kumar, R., Rathore, H., and Singh, J. Joule heating effect on radiating mhd mixed convection stagnation point flow along vertical stretching sheet embedded in a permeable medium and heat generation/absorption. *Heat Transfer 51*, 8 (2022), 7369–7386.

[17] Mondal, S., Oyelakin, I., and Sibanda, P. Unsteady mhd three-dimensional casson nanofluid flow over a porous linear stretching sheet with slip condition. *Frontiers in heat and mass transfer (FHMT) 8* (2017).

[18] Nadeem, S., Haq, R. U., Akbar, N. S., and Khan, Z. H. Mhd three-dimensional casson fluid flow past a porous linearly stretching sheet. *Alexandria Engineering Journal 52*, 4 (2013), 577–582.

[19] Nayak, M., Mahanta, G., Karmakar, K., Mohanty, P., and Shaw, S. Effects of thermal radiation and stability analysis on mhd stagnation casson fluid flow over the stretching surface with slip velocity. In *AIP Conference Proceedings* (2022), vol. 2435, AIP Publishing.

[20] Patel, H. R. Effects of heat generation, thermal radiation, and hall current on mhd casson fluid flow past an oscillating plate in porous medium. *Multiphase Science and Technology 31*, 1 (2019).

[21] Raju, C., and Sandeep, N. Unsteady three-dimensional flow of casson–carreau fluids past a stretching surface. *Alexandria Engineering Journal 55*, 2 (2016), 1115–1126.

[22] Reddy, J. R., Sugunamma, V., and Sandeep, N. Enhanced heat transfer in the flow of dissipative non-newtonian casson fluid flow over a convectively heated upper surface of a paraboloid of revolution. *Journal of Molecular liquids 229* (2017), 380–388.

[23] Reddy, Y. D., Goud, B. S., Chamkha, A. J., and Kumar, M. A. Influence of radiation and viscous dissipation on mhd heat transfer casson nanofluid flow along a nonlinear stretching surface with chemical reaction. *Heat Transfer 51*, 4 (2022), 3495–3511.

[24] Shankar, D. G., Raju, C., Kumar, M. J., and Makinde, O. D. Cattaneo-christov heat flux on an mhd 3d free convection casson fluid flow over a stretching sheet. *Engineering Transactions 68*, 3 (2020), 223–238.

[25] Shatnawi, T. A., Abbas, N., and Shatanawi, W. Comparative study of casson hybrid nanofluid models with induced magnetic radiative flow over a vertical permeable exponentially stretching sheet. *AIMS Math 7*, 12 (2022), 20545–20564.

[26] Singh, J., Kumar, D., Baleanu, D., et al. A hybrid analytical algorithm for thin film flow problem occurring in non-newtonian fluid mechanics. *Ain Shams Engineering Journal 12*, 2 (2021), 2297–2302.

[27] Sobamowo, M., et al. Combined effects of thermal radiation and nanoparticles on free convection flow and heat transfer of casson fluid over a vertical plate. *International Journal of Chemical Engineering 2018* (2018).

[28] Srinivas, S., Kumar, C. K., and Reddy, A. S. Pulsating flow of casson fluid in a porous channel with thermal radiation, chemical reaction and applied magnetic field. *Nonlinear Analysis: Modelling and Control 23*, 2 (2018), 213–233.

[29] Sulochana, C., Ashwinkumar, G., and Sandeep, N. Similarity solution of 3d casson nanofluid flow over a stretching sheet with convective boundary conditions. *Journal of the Nigerian Mathematical Society 35*, 1 (2016), 128–141.

[30] Ullah, I., Khan, I., and Shafie, S. Soret and dufour effects on unsteady mixed convection slip flow of casson fluid over a nonlinearly stretching sheet with convective boundary condition. *Scientific Reports 7*, 1 (2017), 1113.

[31] Yanala, D. R., Kumar, M. A., Bejawada, S. G., Nisar, K. S., Raju, R. S., and Rao, V. S. Exploration of heat and mass transfer on 3-d radiative mhd casson fluid flow over a stretching permeable sheet with chemical reaction. *Case Studies in Thermal Engineering 51* (2023), 103527.